THE JOURNAL OF PHYSICAL CHEMISTRY Letters

Letter

Cite This: J. Phys. Chem. Lett. 2019, 10, 3205−3211

pubs.acs.org/JPCL

Electroabsorption Spectroscopy as a Tool for Probing Charge Transfer and State Mixing in Thermally Activated Delayed Fluorescence Emitters

Daniel de Sa Pereira,[†] Christopher Menelaou,[†] Andrew Danos,[†] Christel Marian,[‡] and Andrew P. Monkman*[,†]

[†]Department of Physics, Durham University, South Road, Durham DH1 3LE, United Kingdom

[‡]Institut für Theoretische Chemie, Heinrich-Heine-Universität, Universitätsstrasse 1, 40225 Düsseldorf, Germany

Supporting Information

ABSTRACT: Solid-state electroabsorption is demonstrated as a powerful tool for probing the charge transfer (CT) character and state mixing in the low-energy optical transitions of two structurally similar thermally activated delayed fluorescent (TADF) materials with divergent photophysical and device performances. The Liptay model is used to fit differentials of the low-energy absorption bands to the measured electroabsorption spectra, with both emitters showing CT characteristics and large changes in dipole moments upon excitation despite the associated absorption bands appearing to be structured. High electric fields then reveal transfer of oscillator strength to a state close to the CT in the better performing molecule. With supporting TDDFT-TDA and DFT/MRCI calculations, this state showed $\pi\pi^*$ characteristics of a local acceptor triplet that strongly mixes with the $\sigma\pi^*$ of the CT. The emitter with poor TADF performance showed no evidence of such mixing.

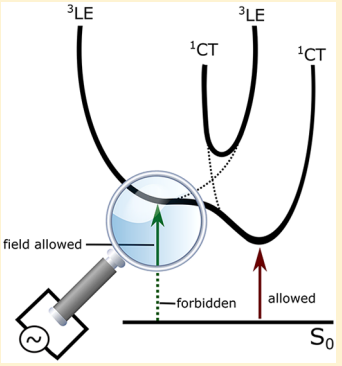

The past few years have seen a great increase in the amount of fundamental and applied research that aimed to exploit thermally activated delayed fluorescent (TADF) molecules for high-efficiency organic light-emitting diodes (OLEDs).[1−3] Via the TADF mechanism, very small singlet−triplet energy gaps (ΔE_{ST}) and vibrational coupling-driven spin−orbit coupling allow the low-energy nonemissive triplet excited states to be up-converted into emissive singlets by reverse intersystem crossing (rISC). This triplet harvesting results in maximum internal quantum efficiencies of ≤100% and external quantum efficiencies as high as 30% in devices, therefore surpassing the limits imposed by spin statistics.[4]

One common design approach for TADF emitters is the linking of electron-donating (D) with electron-accepting (A) units in various combinations (D−A, D−A−D, etc.),[4−7] through a N−C bridging bond between D and A. In these systems, the D and A units then tend to orient perpendicular to one another to decrease the steric energy. This induces a spatial separation of the highest occupied molecular orbital (HOMO) and lowest unoccupied molecular orbital (LUMO). Upon photoexcitation, this leads to the formation of charge transfer singlet (^{1}CT) states with minimal ΔE_{ST}. Works by Monkman et al. and Penfold et al. have demonstrated that while spin−orbit coupling between ^{1}CT and the CT triplet (^{3}CT) state is forbidden, vibronic coupling between ^{3}CT and a local excited triplet (^{3}LE, either D or A) state can mediate the spin flip back to ^{1}CT.[8,9] Marian et al. have also demonstrated that a Frenkel exciton, or an excited local triplet state with a $\pi\pi^*$ character, mediates the transition to the CT state with $n\pi^*$ or $\sigma\pi^*$ character.[10,11] Gaining a better understanding of the precise nature of the electronic excited states and their mutual interactions in TADF systems can thus reveal inherent phenomena and design rules that may not be otherwise evident. Most spectroscopic characterization techniques are limited to investigating direct optically allowed transitions. To probe forbidden transitions and excited-state interactions, however, we rely almost exclusively on sophisticated theoretical modeling and calculations. In contrast, electroabsorption (EA) spectroscopy provides direct information about the character of relevant excited states and their interactions in a simple and relatively inexpensive manner.[12−15] On the basis of the Stark effect, EA measures changes in absorption caused by a perturbing external electric field, in particular peak shifts and line shape changes. Because it is an optical absorption technique (strictly third-order nonlinear susceptibility), only instantaneous changes are determined. This means that all excited-state effects, such as relaxation after excitation through interactions with a polar host environment, can be avoided as they have a response time of many nanoseconds after photogeneration of the excited state. Electrofluorescence (EF) measurements on the other hand, could provide information about the tuning effect of the CT states with the polarity of the host chosen for measurements, especially if time-resolved EF could be achieved, adding an

Received: April 8, 2019
Accepted: May 21, 2019
Published: May 22, 2019

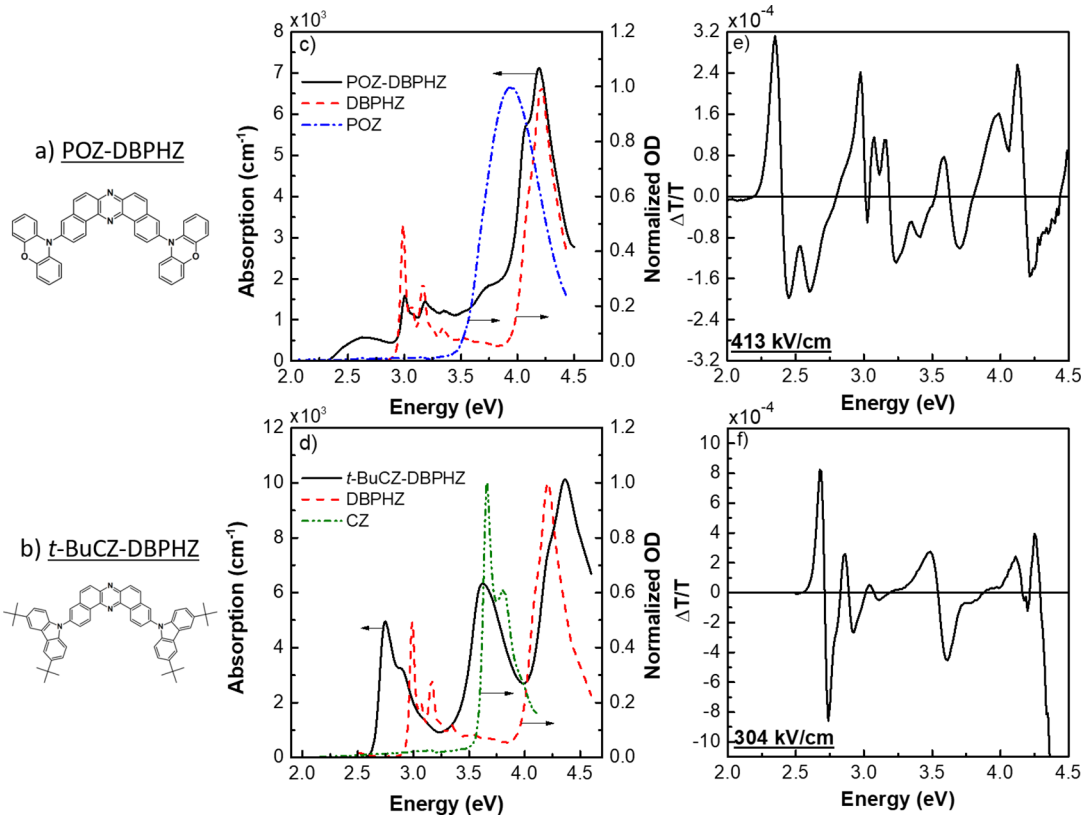

Figure 1. Electroabsorption (EA) spectroscopy of two structurally similar emitters with diverging TADF properties: (a) POZ-DBPHZ and (b) *t*-BuCZ-DBPHZ. The absorption coefficients are shown in panels c and d for each emitter and overlapped with the absorption of the DBPHZ core (red dashed line), POZ (blue dotted−dashed line), and Carbazole (Cz, green dotted−dotted−dashed line). Finally, the EA spectra at (e) 95 V and (f) 70 V are also shown. It is worth mentioning the difference in scales as they are different between the two materials. Measurements collected in emitter-in-zeonex blends with a layer thickness of 2.3 μm, determined with a profilometer.

extra degree of complexity to sample production, data collection, and interpretation. In this sense, the EA measurement is simple and free of complications associated with such excited-state relaxation processes and is the basis for this initial study.[8] In this sense, moreover, these changes in absorption allow determination of parameters such as the change in the electric dipole moment ($\Delta\mu$) and polarizability $\Delta\alpha$ upon excitation caused by the perturbing field, as well as the character of the excited states formed on optical transitions. Details about the calculation of these parameters are presented in section S1 of the Supporting Information. EA therefore becomes particularly interesting for determining the origin of different types of excitons (such as Frenkel or CT) in TADF.[16,17]

In this study, we have measured the solid-state EA spectra of two D−A−D materials with a common dibenzo[*a*,*j*]phenazine (DBPHZ) A core and either phenoxazine (POZ) or *tert*-butylcarbazole (*t*-BuCZ) D units. POZ-DBPHZ (Figure 1a) was previously found to give good TADF and device performances (maximum η_{ext} of 16% in the orange)[18] as well as complex mechanochromic properties.[19,20] In contrast, *t*-BuCZ-DBPHZ (Figure 1b) has much weaker TADF and OLED performance, ∼8%. This pair of emitters was therefore chosen due to their similar structures (sharing the same acceptor core) yet distinct TADF properties. Legaspi et al. report both EA and EF for two TADF molecules in a (frozen) solvent observing strong charge transfer character on the red edge of the absorption band and higher local transitions. A field-dependent contribution to EA was observed in one molecule and suggested that potential mixing of the lowest-lying absorption bands with neighboring states without connecting it to their TADF performance.[16] In this study, however, we use EA in the solid state to understand further how the differences in molecular structure, energy levels, and state mixing lead to divergent TADF and device performances in two TADF molecules with a common acceptor core. We analyze in detail the low-energy absorption bands of both and confirm their high dipole moment by fitting the zeroth, first, and second differentials of the their absorption spectra to the EA spectra in a typical Liptay analysis.[21] Both materials show very strong second-order features at the onset of absorption, indicative of CT transitions. In POZ-DBPHZ, we discover—through transfer of oscillator strength and supported by TDDFT-TDA and DFT/MRCI calculations and time-resolved spectroscopy measurements—a state lying close in energy to the CT state with a local character (Frenkel exciton). We propose that this provides direct evidence of a mixed $\pi\pi^*$ triplet local state with a strong $\sigma\pi^*$ CT transition in POZ-DBPHZ and is a strong indicator of TADF efficiency. In contrast, *t*-BuCZ-DBPHZ does not show such mixing, which correlates with it being a much weaker TADF material.

As is common in intramolecular CT molecules, the absorption spectrum is a superposition of D and A unit absorption indicating the effective electronic decoupling required for charge transfer.[22] Therefore, in the absorption of POZ-DBPHZ (Figure 1c), we attribute the peaks above 4 eV and between 2.9 and 3.5 eV to the $\pi\pi^*$ absorptions observed in the pure dibenzo[*a*,*j*]phenazine A along with a slight contribution from the $\pi\pi^*$ absorption of the phenoxazine

DOI: 10.1021/acs.jpclett.9b00999
J. Phys. Chem. Lett. 2019, 10, 3205−3211

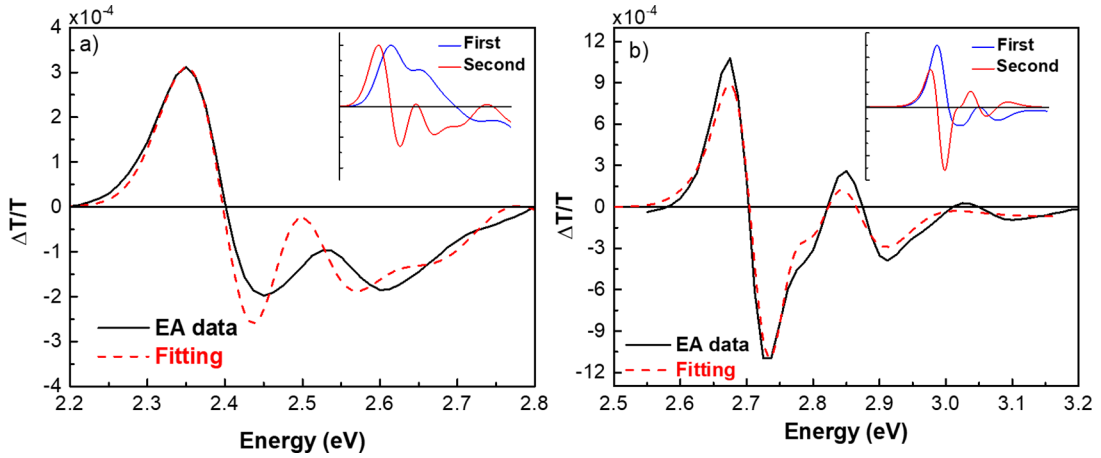

Figure 2. Low-energy electroabsorption band (solid black line) spectra of (a) POZ-DBPHZ and (b) *t*-BuCZ-DBPHZ overlapped with the fitting (dashed red line). For comparison, the insets of both figures show the first and second derivatives of the lowest-energy absorption bands calculated from the Gaussian reconstruction (Figure S2).[27]

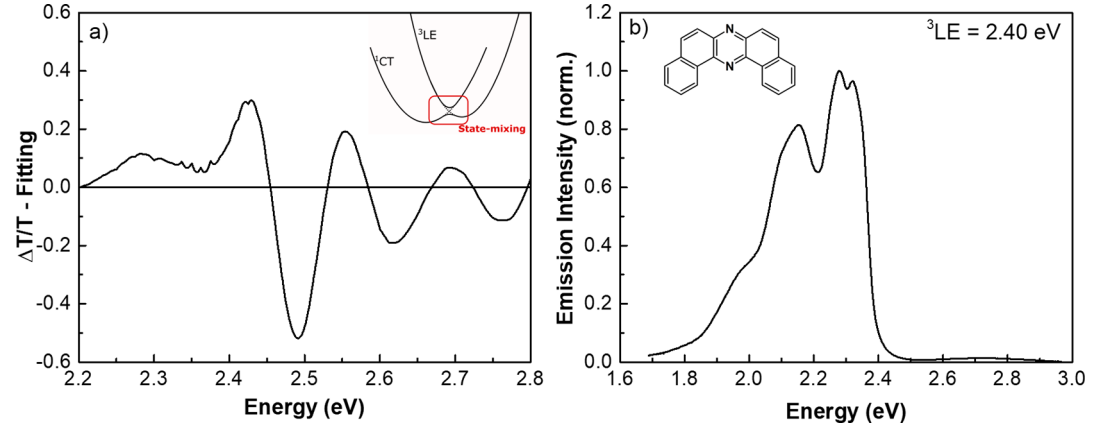

Figure 3. (a) Difference between the raw and fitted EA spectrum of POZ-DBPHZ in a zeonex matrix. The inset shows a theoretical diagram of the state mixing between ^{1}CT and ^{3}LE that results in the transfer of oscillator strength to the ^{3}LE state, thus allowing the state to be probed by EA measurements. (b) Normalized phosphorescence spectrum of DBPHZ (molecular structure shown in the inset) obtained with time-resolved measurements in a blend of 1% (w:w) DBPHZ in zeonex and a time delay above 25 ms. Onset measurement gives a state energy of 2.40 ± 0.02 eV.

D between 3.5 and 4 eV. At low energies, in POZ-DBPHZ we observe the appearance of an extra band, with a Gaussian line shape, which we assign to a direct CT absorption band, typical of D−A−D systems.[3,6,23]

In POZ-DBPHZ, X-ray crystal structures[18] show the D−A dihedral angles are very close to 90° in the ground state, whereas in *t*-BuCZ-DBPHZ, the angles are around 60°, very typical of carbazole donors.[24] This will result in an increased level of π delocalization across the D−A bond, and therefore, the lowest-energy transition in *t*-BuCZ-DBPHZ (Figure 1d) should therefore have far more local exciton character[25] and hence an oscillator strength greater than that of the CT transition in POZ-DBPHZ. This transition does indeed appear more like the DBPHZ acceptor absorption with a weak CT character rather than a wholly new, direct CT absorption feature. We also note that with carbazole, the nonbonding n electrons delocalize into the carbazole ring, potentially limiting the formation of a direct CT transition below the DBPHZ absorption. In POZ-DBPHZ, the A absorption is not shifted (Figure 1a) and peaks at 3 eV just as the pure DBPHZ does, but we also observe a strong new direct CT transition below this. In *t*-BuCZ-DBPHZ (Figure 1b), the conjugated DBPHZ band red-shifts and sits above any weak direct CT absorption that might be present.

The EA spectra of both POZ-DBPHZ and *t*-BuCZ-DBPHZ are also shown in panels e and f of Figure 1, respectively. The spectra are characterized by high-intensity and low-energy EA bands and high-energy bands that we suspect originate in the D and A. At higher energies, the spectra are complex and cannot be described well using Liptay analysis,[21] which assumes a series of non-interacting excited states (and their associated transitions) and cannot take into consideration optically forbidden states that do not feature in the absorption spectrum. As a result, a simple Liptay model assuming separate D and A responses cannot reproduce the entire spectrum. As one can see in Figure 1, the full EA spectrum of POZ-DBPHZ is far more complex than that of *t*-BuCZ-DBPHZ, and evidence of strong state mixing and transfer of oscillator strength across the whole $\pi\pi^*$ spectral region can be seen. A more comprehensive sum-over-states model may be able to describe this high-energy region,[26] but fitting such complex spectra was deemed beyond the scope of this initial study.

As the performance of TADF materials is determined by the behavior of the low-lying CT states,[2] we focus our analysis on the low-energy absorption bands that can be fitted well by the

DOI: 10.1021/acs.jpclett.9b00999
J. Phys. Chem. Lett. 2019, 10, 3205−3211

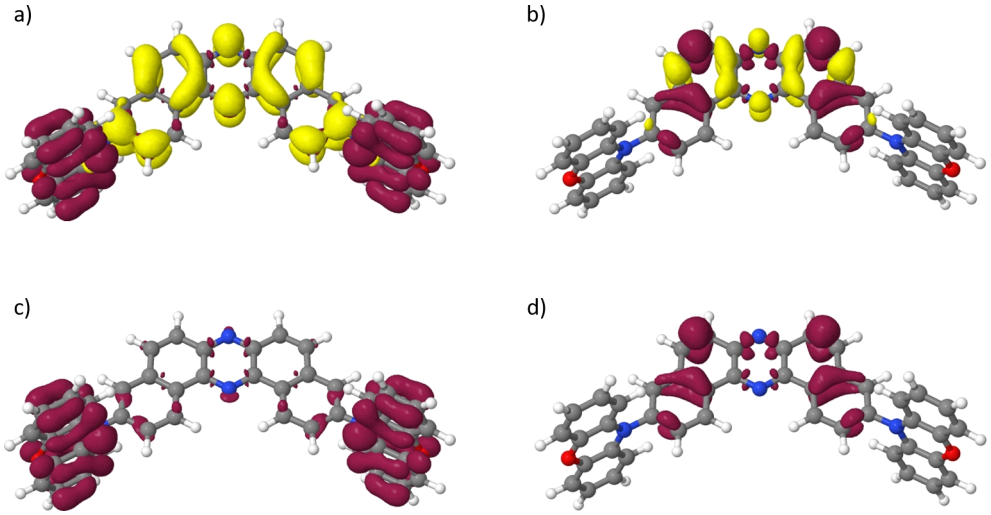

Figure 4. Difference densities (lisovaluel = 0.001) of (a) the S_1(CT) state and (b) the $T_3(\pi\pi^*)$ state of POZ-DBPHZ. A loss of electron density with respect to the ground state is colored red, and a gain yellow. For the sake of clarity, the negative parts of the corresponding difference densities are shown in panels c and d, respectively.

Liptay model. These bands are overlapped with the EA bands and show a general red-shift, which is more pronounced in POZ-DBPHZ (Figure S1). As described in Methods, the absorption bands of both molecules below 3.2 eV were reconstructed with a set of Gaussian components as shown in Figure S2 to obtain smooth, noise free derivatives following numerical differentiation. Using the analytic derivatives of the fitted Gaussians, the first and second differentials of the low-energy absorption spectra were then calculated (insets of Figure 2). Least-squares fitting using zeroth, first, and second differential components allows the EA spectra to be fitted using eq 2 from section S1 of the Supporting Information, and the results are shown in Figure 2.

At first glance, the EA spectra of both POZ-DBPHZ (a) and *t*-BuCZ-DBPHZ (b) are dominated by second-derivative contributions, revealing strong CT character in the lowest-energy absorption bands in both. POZ-DBPHZ (Figure 2a) cannot be fit entirely well (particularly in the region above 2.45 eV), suggesting additional contributions from other states that overlap with the main CT electroabsorption band. The *t*-BuCZ-DBPHZ EA spectrum in comparison is reproduced very well and is almost a pure second-order response showing that, contrary to what we first assumed, this transition is indeed CT in origin with high LE character (Figure 2b). A CT transition with greater LE character also possesses a higher oscillator strength, which explains how *t*-BuCZ-DBPHZ has a signal-to-noise ratio that is ∼3 times higher than that of POZ-DBPHZ at a lower applied field (304 kV/cm vs 413 kV/cm).

In POZ-DBPHZ, via examination of the fit residuals, a new feature is revealed at around 2.45 eV, shown in Figure 3a.[28] The perturbing electric field causes coupling of a dark state to an allowed transition, leading to the transfer of oscillator strength.[29] A derivative-like feature with strong first-order differential character is observed, spanning 2.35 and 2.6 eV and centered around 2.49 eV. We assign this non-Liptay new feature to the triplet exciton located on the acceptor that becomes optically allowed through coupling to the CT singlet state and confirmed by the measured phosphorescence spectrum of the DBPHZ core (Figure 3b), from which an onset energy of 2.40 eV is obtained. This energy matches well that observed in the EA spectrum and is substantially removed from the lowest singlet states lying on either the donor or the acceptor units, all of which lie above 3 eV. These observations are further confirmed by the DFT/MRCI calculations described in detail in the section S2 of the Supporting Information. In POZ-DBPHZ, the lowest-energy optical transitions for the full molecule (1^1B_1 and 1^1A_2) both have pure CT character with calculated adiabatic transition energies of 2.29 eV, in excellent agreement with the measured onset of optical absorption (Figure 1). The lowest singlet local transitions (of the acceptor) are calculated at 2.95 and 3.22 eV, strongly separated from the CT transitions. The triplet state mentioned above is calculated to be a local 1^3B_1 triplet state of $\pi\pi^*$ character, localized on the acceptor. With a calculated energy of 2.32 eV, this is in close agreement with the values observed in the EA and phosphorescence measurements (Table S3).

The first-order line shape of the EA associated with this underlying transition, centered at 2.45 eV, must be a Frenkel excitonic state on a single unit spectrally overlapping with the CT feature in the EA spectrum. Previous solvatochromism measurements[18] have shown that the CT transition has strong mixed $n\pi^*/\pi\pi^*$ character, and the applied field allows this mixing to become measurable. While direct excitation to this state is forbidden, the transition becomes visible in the EA spectrum through the transfer of oscillator strength. This is also in agreement with El-Sayed's rule, which states that an $S(\pi\pi^*)$ state couples strongly with a $T(n\pi^*)$ or $T(\sigma\pi^*)$ state and vice versa.[30] In essence, spin−orbit coupling is expected to be strong if the p orbital at an atomic center changes its orientation upon excitation. The different densities of the CT states (Figure 4) reveal small local $\sigma\pi^*$-type contributions to the CT excitations that may couple to the $\pi\pi^*$-type excitations of the $T_3(\pi\pi^*)$ state on the same center. The computed spin−orbit coupling matrix element between the energetically close-lying S_1(CT) and $T_3(\pi\pi^*)$ states (0.279 cm^{-1}) is ∼50 times stronger than the direct symmetry-allowed coupling between S_1(CT) and T_2(CT). The effects of such state mixing have been discussed in detail by Marian et al. and strongly influence the TADF mechanism[11] but on their own are still orders of magnitude too small to account for the observed experimental rISC rates, which require the vibronic coupling mechanism to

DOI: 10.1021/acs.jpclett.9b00999
J. Phys. Chem. Lett. 2019, 10, 3205−3211

Table 1. Contributions of First and Second Derivatives to the Fitting of the EA Spectra of POZ-DBPHZ and *t*-BuCZ-DBPHZ[a]

	first-derivative contribution × 10^{-5}	$\Delta p \times 10^{-38}$ (Dm/V)	$\Delta p \times 10^{-38}$ (Dm/V)[b]	second-derivative contribution × 10^{-5}	$\Delta\mu$ (D)	$\Delta\mu$ (D)[b]
POZ-DBPHZ	5.3	1.05	0.29	3.8	17.46	9.35
t-BuCZ-DBPHZ	−2.7	−0.94	−0.27	0.3	6.25	3.35

[a]Following eqs 3 and 4, the field-induced change in polarizability and dipole moment were calculated. [b]Corrected for a nonpolar environment using a local field correction factor of $F = (2\varepsilon + 1)F_{app}/3$.

achieve rISC rates approaching 10^7 s^{-1}.[4] Thus, EA gives experimental verification that the lowest-lying optical transition in POZ-DBPHZ is a pure CT transition but one that couples (mixes) with the lowest-energy local triplet state. Given this triplet state is $\pi\pi^*$ in character, the CT transition has to be (as predicted) $\sigma\pi^*$ and the mixing of the two states yields enhanced transition oscillator strength for the otherwise optically inaccessible state.

In comparison, DFT/MRCI calculations show that *t*-BuCZ-DBPHZ (also with pure CT character) has no such triplet-state coupling to the lowest-energy optical transition (Table S5). The lowest-energy triplet state from phosphorescence and DFT/MRCI has an energy of ∼2.30 eV, well below the CT states and far removed from any EA signal, so no major deviation from the pure second-order derivative line shape is seen in the EA spectrum. We note that though this transition in *t*-BuCZ-DBPHZ seems at first glance excitonic (being sharp and well featured), EA clearly shows that this transition is pure CT in character. We speculate whether this is a peculiar characteristic of the carbazole donor and stems from the fact that the nonbonding electrons are delocalized into the carbazole ring.

In Table 1, we summarize the changes in polarizability and dipole moment of these two materials, using eqs 3 and 4 of section S1 of the Supporting Information both with and without a local field correction. POZ-DBPHZ, having both the smallest ΔE_{ST} and the highest PLQY, also shows a large change in dipole moment ($\Delta\mu$) of 17.46 D (uncorrected). This change is indicative of a complete one-electron transfer over a distance of 5−7 Å, which we suggest represents one electron moving from the donor unit into the middle of the acceptor unit. Such a change in electron density is also confirmed by DFT/MRCI calculations of the first CT transitions (Table S3). We also see a change in the first-order polarizability indicating the transfer of oscillator strength to the local acceptor S_0-T_1 transition. In the case of *t*-BuCZ-DBPHZ, the change in dipole moment is smaller, calculated at 6.25 D. We attribute this smaller $\Delta\mu$ to the smaller dihedral angle in *t*-BuCZ-DBPHZ and the conjugation of the donor and acceptor units to some degree. Conjugation and associated ground-state delocalization across the D and A units reduce the distance the electron must travel in forming the CT state, resulting in a smaller change in dipole moment upon excitation. Even with the weaker CT character and increased level of D−A conjugation, *t*-BuCZ-DBPHZ has a smaller PLQY. This and the large ΔE_{ST} (of 0.33 eV) result in poor TADF efficiency and give low-efficiency devices. These properties could be a direct result of a lack of mixing of CT and LE states in this molecule. Correcting the applied field for the nonpolar zeonex host reduces the calculated change in dipole moment. The resulting values seem rather unphysical for such strong charge transfer molecules that show very large solvatochromic shifts.[16] We feel that 5% (w:w) loading of the polar TADF molecules in zeonex may well create a polar environment and a different local field correction factor needs to be used. However, all corrections we have tried greatly increase the calculated change in dipole moment, again to nonphysical values. Further studies to fully understand the interaction of the TADF guest in a host medium need to be performed to resolve this. EA spectroscopy is then a powerful tool for predicting efficient TADF in materials for OLEDs, as it quickly reveals the presence or absence of this important CT−LE mixing.

Conclusions. In summary, we have elucidated the character and state mixing of the molecular excited states of two distinct TADF materials using electroabsorption spectroscopy. We find that the low-energy absorption bands in both have very strong CT character, which is not obvious from the absorption line shape of *t*-BuCZ-DBPHZ. More importantly, in POZ-DBPHZ, the transfer of oscillator strength reveals the presence of a second state that is overlapping the CT band and is not found in *t*-BuCZ-DBPHZ that has pure CT character. This new state in POZ-DBPHZ is identified as the lowest-energy $\pi\pi^*$ local triplet of the acceptor. With support from calculations and further spectroscopic techniques, this local triplet state is shown to mix with the $\sigma\pi^*$ CT state. The computed spin−orbit coupling matrix element (0.279 cm^{-1}) is ∼50 times stronger than the direct and symmetry-allowed coupling between $S_1(CT)$ and $T_2(CT)$. This mixing gives a direct CT transition with an enhanced oscillator strength. In *t*-BuCZ-DBPHZ, the lowest triplet state is much lower in energy than the CT transition and does not mix, in part leading to much poorer TADF efficiency. No higher-lying local triplet states are in resonance either. This may be a peculiarity of the carbazole donors in *t*-BuCZ-DBPHZ. Further studies of this CT singlet−LE triplet coupling with quantum chemistry approaches may well yield more details of the molecular characteristics that result in efficient TADF molecules.

METHODS

For absorption and electroabsorption (EA) measurements, samples of ∼7 mg of POZ-DBPHZ and *t*-BuCZ-DBPHZ dispersed in 1 mL of toluene with ∼143 mg of zeonex [1:20 (w:w) ratio] were used. For EA, sapphire substrates were loaded into a Kurt J. Lesker Spectros II vacuum thermal deposition chamber and layers of aluminum were evaporated at a pressure of $\leq 10^{-5}$ mbar. After the initial evaporation of a 9 nm electrode, covering the entire substrate, around 70 μL of the solution was spun for 30 s and 2000 rpm using a Laurell Technologies spin-coater, resulting in a film thickness of approximately 2.3 ± 0.1 μm, which was confirmed by a DekTac profilometer. The samples were then reloaded into the chamber, and a further 12 nm thick Al layer was deposited, where only part of the substrate was evaporated, to facilitate connection to the bottom Al layer. Electrical contacts were made using silver paste to connect electrodes to electrical wires. For absorption, the same solution and spin-coating parameters were used with blank sapphire substrates.

DOI: 10.1021/acs.jpclett.9b00999
J. Phys. Chem. Lett. 2019, 10, 3205−3211

Absorption spectra were measured with a double-beam spectrophotometer (Shimadzu UV-3600). For time-resolved measurements, toluene solutions of DBPHZ (at a concentration of 1 mg/mL) and zeonex (at a concentration of 130 mg/mL) were blended in a ratio of 1:1 (w:w) and drop-cast (~90 μL) at room temperature onto similar sapphire substrates. Time-resolved phosphorescence was collected by exciting the sample with a Nd:YAG laser (EKSPLA, 10 Hz, 266 nm) and recorded using a Stanford Computer Optics gated charged coupled device (CCD) with a time delay above 25 ms.

EA spectra were recorded using a home-built system (Figure S9) comprising a laser-driven white light source (Energetiq EQ-99X) focused before the sample to prevent sample burn-in. The transmitted beam was passed through a monochromator (Bentham TMc300) and measured with a silicon photodiode. The voltage to set up the electric field was supplied by a Trek 10/10 voltage amplifier, capable of amplifying the sinusoidal internal oscillator signal (f = 173 Hz) of a DSP 7225 lock-in amplifier by 1000 times. Considering the total film thickness and applied voltage, maximum electric fields of 413 and 304 kV/cm were used for POZ-DBPHZ and t-BuCZ-DBPHZ, respectively. We repeatedly found that higher voltages and fields rapidly damaged the contacts, increasing the chance of sample failure midmeasurement. The field-induced change in transmission (ΔT) and the nominal transmission (T) were detected by the photodiode connected to the lock-in amplifier at specific monochromator wavelengths. This in turn provided the energy dispersion of $\Delta T/T$.

■ ASSOCIATED CONTENT

Supporting Information

The Supporting Information is available free of charge on the ACS Publications website at DOI: 10.1021/acs.jpclett.9b00999.

Details on Stark spectral analysis, DFT/MRCI calculations, and experimental setup (PDF)

■ AUTHOR INFORMATION

Corresponding Author

*E-mail: a.p.monkman@durham.ac.uk.

ORCID

Daniel de Sa Pereira: 0000-0002-5784-2124
Andrew Danos: 0000-0002-1752-8675
Christel Marian: 0000-0001-7148-0900
Andrew P. Monkman: 0000-0002-0784-8640

Notes

The authors declare no competing financial interest.

■ ACKNOWLEDGMENTS

The authors acknowledge the EXCILIGHT project funded by the European Union's Horizon 2020 Research and Innovation Programme under Grant Agreement 674990. This work was also supported by EPSRC Grant EP/L02621X/1 and the European Union's Horizon 2020 research and innovation programme, HyperOLED, under Grant Agreement 732013. C. Marian acknowledges financial support by the Deutsche Forschungsgemeinschaft (DFG) through Project MA-1051/17-1.

■ REFERENCES

(1) Uoyama, H.; Goushi, K.; Shizu, K.; Nomura, H.; Adachi, C. Highly Efficient Organic Light-Emitting Diodes from Delayed Fluorescence. *Nature* **2012**, *492* (7428), 234−238.

(2) Dias, F. B.; Penfold, T. J.; Monkman, A. P. Photophysics of Thermally Activated Delayed Fluorescence Molecules. *Methods Appl. Fluoresc.* **2017**, *5* (1), 012001.

(3) Dias, F. B.; Bourdakos, K. N.; Jankus, V.; Moss, K. C.; Kamtekar, K. T.; Bhalla, V.; Santos, J.; Bryce, M. R.; Monkman, A. P. Triplet Harvesting with 100% Efficiency by Way of Thermally Activated Delayed Fluorescence in Charge Transfer OLED Emitters. *Adv. Mater.* **2013**, *25* (27), 3707−3714.

(4) dos Santos, P. L.; Ward, J. S.; Congrave, D. G.; Batsanov, A. S.; Eng, J.; Stacey, J. E.; Penfold, T. J.; Monkman, A. P.; Bryce, M. R. Triazatruxene: A Rigid Central Donor Unit for a D-A 3 Thermally Activated Delayed Fluorescence Material Exhibiting Sub-Microsecond Reverse Intersystem Crossing and Unity Quantum Yield via Multiple Singlet-Triplet State Pairs. *Adv. Sci.* **2018**, *5* (6), 1700989.

(5) Cui, L. S.; Nomura, H.; Geng, Y.; Kim, J. U. k.; Nakanotani, H.; Adachi, C. Controlling Singlet−Triplet Energy Splitting for Deep-Blue Thermally Activated Delayed Fluorescence Emitters. *Angew. Chem., Int. Ed.* **2017**, *56* (6), 1571−1575.

(6) dos Santos, P. L.; Ward, J. S.; Bryce, M. R.; Monkman, A. P. Using Guest−Host Interactions To Optimize the Efficiency of TADF OLEDs. *J. Phys. Chem. Lett.* **2016**, *7* (17), 3341−3346.

(7) Oh, C. S.; Lee, H. L.; Han, S. H.; Lee, J. Y. Rational Molecular Design Overcoming the Long Delayed Fluorescence Lifetime and Serious Efficiency Roll-Off in Blue Thermally Activated Delayed Fluorescent Devices. *Chem. - Eur. J.* **2019**, *25* (2), 642−648.

(8) Gibson, J.; Penfold, T. J. Nonadiabatic Coupling Reduces the Activation Energy in Thermally Activated Delayed Fluorescence. *Phys. Chem. Chem. Phys.* **2017**, *19* (12), 8428−8434.

(9) Etherington, M. K.; Gibson, J.; Higginbotham, H. F.; Penfold, T. J.; Monkman, A. P. Revealing the Spin−vibronic Coupling Mechanism of Thermally Activated Delayed Fluorescence. *Nat. Commun.* **2016**, *7* (1), 13680.

(10) Marian, C. M. Mechanism of the Triplet-to-Singlet Upconversion in the Assistant Dopant ACRXTN. *J. Phys. Chem. C* **2016**, *120* (7), 3715−3721.

(11) Lyskov, I.; Marian, C. M. Climbing up the Ladder: Intermediate Triplet States Promote the Reverse Intersystem Crossing in the Efficient TADF Emitter ACRSA. *J. Phys. Chem. C* **2017**, *121* (39), 21145−21153.

(12) Boxer, S. G. Stark Realities. *J. Phys. Chem. B* **2009**, *113* (10), 2972−2983.

(13) Iimori, T.; Ito, R.; Ohta, N.; Nakano, H. Stark Spectroscopy of Rubrene. I. Electroabsorption Spectroscopy and Molecular Parameters. *J. Phys. Chem. A* **2016**, *120* (25), 4307−4313.

(14) Yanagi, K.; Gardiner, A. T.; Cogdell, R. J.; Hashimoto, H. Electroabsorption Spectroscopy of β -Carotene Homologs: Anomalous Enhancement of $\Delta\mu$. *Phys. Rev. B: Condens. Matter Mater. Phys.* **2005**, *71* (19), 195118.

(15) Pedrolli, D. B.; Jankowitsch, F.; Schwarz, J.; Langer, S.; Nakanishi, S.; Mack, M. Flavins and Flavoproteins. *Methods Mol. Biol.* **2014**, *1146*, 455−463.

(16) Legaspi, C. M.; Stubbs, R. E.; Wahadoszaman, M.; Yaron, D. J.; Peteanu, L. A.; Kemboi, A.; Fossum, E.; Lu, Y.; Zheng, Q.; Rothberg, L. J. Rigidity and Polarity Effects on the Electronic Properties of Two Deep Blue Delayed Fluorescence Emitters. *J. Phys. Chem. C* **2018**, *122*, 11961−11972.

(17) Feller, F.; Monkman, A. Optical Spectroscopy of Oriented Films of Poly(2,5-Pyridinediyl). *Phys. Rev. B: Condens. Matter Mater. Phys.* **2000**, *61* (20), 13560−13564.

(18) Data, P.; Pander, P.; Okazaki, M.; Takeda, Y.; Minakata, S.; Monkman, A. P. Dibenzo[a,j]Phenazine-Cored Donor-Acceptor-Donor Compounds as Green-to-Red/NIR Thermally Activated Delayed Fluorescence Organic Light Emitters. *Angew. Chem., Int. Ed.* **2016**, *55* (19), 5739−5744.

DOI: 10.1021/acs.jpclett.9b00999
J. Phys. Chem. Lett. 2019, 10, 3205−3211

(19) Pereira, D. de S.; Dos Santos, P. L.; Ward, J. S.; Data, P.; Okazaki, M.; Takeda, Y.; Minakata, S.; Bryce, M. R.; Monkman, A. P. An Optical and Electrical Study of Full Thermally Activated Delayed Fluorescent White Organic Light-Emitting Diodes. *Sci. Rep.* **2017**, *7* (1), 6234.
(20) Okazaki, M.; Takeda, Y.; Data, P.; Pander, P.; Higginbotham, H.; Monkman, A. P.; Minakata, S. Thermally Activated Delayed Fluorescent Phenothiazine−dibenzo[a,j]Phenazine−phenothiazine Triads Exhibiting Tricolor-Changing Mechanochromic Luminescence. *Chem. Sci.* **2017**, *8* (4), 2677−2686.
(21) Liptay, W. Dipole Moments and Polarizabilities of Molecules in Excited Electronic States. In *Excited States*; Elsevier, 1974; Vol. *1*, pp 129−229.
(22) Dias, F. B.; Santos, J.; Graves, D. R.; Data, P.; Nobuyasu, R. S.; Fox, M. A.; Batsanov, A. S.; Palmeira, T.; Berberan-Santos, M. N.; Bryce, M. R.; et al. The Role of Local Triplet Excited States and D-A Relative Orientation in Thermally Activated Delayed Fluorescence: Photophysics and Devices. *Adv. Sci.* **2016**, *3* (12), 1600080.
(23) Santos, P. L.; Ward, J. S.; Data, P.; Batsanov, A. S.; Bryce, M. R.; Dias, F. B.; Monkman, A. P. Engineering the Singlet−triplet Energy Splitting in a TADF Molecule. *J. Mater. Chem. C* **2016**, *4* (17), 3815−3824.
(24) Oh, C. S.; Pereira, D. D. S.; Han, S. H.; Park, H.-J.; Higginbotham, H. F.; Monkman, A. P.; Lee, J. Y. Dihedral Angle Control of Blue Thermally Activated Delayed Fluorescent Emitters through Donor Substitution Position for Efficient Reverse Intersystem Crossing. *ACS Appl. Mater. Interfaces* **2018**, *10* (41), 35420−35429.
(25) Al-Attar, H. A.; Griffiths, G. C.; Moore, T. N.; Tavasli, M.; Fox, M. A.; Bryce, M. R.; Monkman, A. P. Highly Efficient, Solution-Processed, Single-Layer, Electrophosphorescent Diodes and the Effect of Molecular Dipole Moment. *Adv. Funct. Mater.* **2011**, *21* (12), 2376−2382.
(26) Saito, K.; Yanagi, K.; Cogdell, R. J.; Hashimoto, H. A Comparison of the Liptay Theory of Electroabsorption Spectroscopy with the Sum-over-State Model and Its Modification for the Degenerate Case. *J. Chem. Phys.* **2011**, *134* (4), 044138.
(27) Oh, D. H.; Sano, M.; Boxer, S. G. Electroabsorption (Stark Effect) Spectroscopy of Mono- and Biruthenium Charge-Transfer Complexes: Measurements of Changes in Dipole Moments and Other Electrooptic Properties. *J. Am. Chem. Soc.* **1991**, *113* (18), 6880−6890.
(28) Leng, J. M.; Jeglinski, S.; Wei, X.; Benner, R. E.; Vardeny, Z. V.; Guo, F.; Mazumdar, S. Optical Probes of Excited States in Poly(p -Phenylenevinylene). *Phys. Rev. Lett.* **1994**, *72* (1), 156−159.
(29) Liess, M.; Jeglinski, S.; Vardeny, Z.; Ozaki, M.; Yoshino, K.; Ding, Y.; Barton, T. Electroabsorption Spectroscopy of Luminescent and Nonluminescent π-Conjugated Polymers. *Phys. Rev. B: Condens. Matter Mater. Phys.* **1997**, *56* (24), 15712−15724.
(30) El-Sayed, M. A. The Triplet State: Its Radiative and Nonradiative Properties. *Acc. Chem. Res.* **1968**, *1* (1), 8−16.

DOI: 10.1021/acs.jpclett.9b00999
J. Phys. Chem. Lett. 2019, 10, 3205−3211